

Discovery of a Young Massive Stellar Cluster associated with IRAS source 16177-5018 ¹

A. Roman-Lopes, Z. Abraham and J. R. D. Lépine

*Instituto de Astronomia, Geofísica e Ciências Atmosféricas, Universidade de São Paulo
Rua do Matão 1226, 05508-900, São Paulo, SP, Brazil*

roman@astro.iag.usp.br

ABSTRACT

We report the discovery of a young massive stellar cluster embedded in an extended HII region, invisible at optical wavelengths where the extinction is $A_V \approx 28$ magnitudes, associated with the IRAS source 16177-5018. J , H and nbK imaging photometry combined with the K_S 2MASS data show the presence of sources with infrared excess emission at $2.2 \mu\text{m}$, concentrated in an area of about one square parsec around a massive young stellar object identified as the IRAS source. This object has a near-mid infrared spectral index between 2.2 and $25 \mu\text{m}$ $\alpha(\text{IR}) = d \log(\lambda F_\lambda) / d \log \lambda = 4.78$, characteristic of compact H II regions, with bolometric luminosity, inferred from the integrated near to far-infrared flux density of $2.8 \times 10^5 L_\odot$, which corresponds to a ZAMS star of about $42 M_\odot$. From the color-magnitude diagram we were able to classify the majority of the cluster members as reddened massive stars earlier than spectral type B5.

Subject headings: stars : formation – stars: pre-main sequence – infrared : stars – ISM: HII regions – ISM: dust, extinction

1. Introduction

Young massive stars are formed in dense giant molecular clouds, where the gas density may be as high as $n_H = 10^5 - 10^6 \text{ cm}^{-3}$ and the temperature as low as $T = 10 - 20 \text{ K}$. For this reason, the star forming regions that eventually lie in the core of the molecular cloud can be completely obscured at optical wavelengths by many magnitudes of extinction. On the other hand, the dense molecular clouds can be traced by molecular emission, like CS and NH₃ lines at radio frequencies, which are powerful tools for the determination of the physical conditions in the clouds. While OB stars are embedded in a molecular cloud, they dissociate and ionize the gas, forming compact HII regions seen at radio wavelengths, and heat the circumstellar dust which eventually radiates most of the

¹Based on observations made at Laboratório Nacional de Astrofísica/MCT, Brazil

stellar luminosity in the far-infrared (FIR). Therefore, the most prominent tracers of young massive stars are also compact, or ultracompact H II (UC H II) regions, which have electron densities greater than 10^4 cm^{-3} and diameters smaller than 0.1 pc. Wood & Churchwell (1989) showed that these ultracompact H II regions have characteristic spectral energy distributions in the far-infrared, occupying a well delimited region in the $\log[F_\nu(60\mu\text{m})/F_\nu(12\mu\text{m})] \times \log[F_\nu(25\mu\text{m})/F_\nu(12\mu\text{m})]$ space. Bronfman et al. (1996) made an extensive survey of the CS (2-1) line emission toward IRAS point sources with colors characteristics of ultra-compact H II regions and Roman-Lopes et al. (2002) detected ammonia emission in the direction of the strongest sources in that survey. With the advent of the large bidimensional near-infrared array detectors, the morphological and photometric studies of extremely young galactic stellar clusters were greatly benefited. At near-infrared wavelengths (1 to $2.5 \mu\text{m}$) it is possible to probe deep into the dense dust clouds where star formation is taking place. At those wavelengths, very young objects present large infrared excess due the presence of warm circumstellar dust.

In this paper we present the discovery of a young stellar cluster of massive stars and its associated HII region, in the direction of the IRAS source 16177-5018. We combined 2MASS (Two Micron All Sky Survey) data with new NIR observations from Laboratório Nacional de Astrofísica (LNA), Brazil. This work is a part of a survey aimed to the identification of stellar populations in the direction of IRAS sources that have colors characteristics of ultracompact HII regions (Wood & Churchwell 1989) and strong CS (2-1) line emission (Bronfman et al. 1996). The studied region is part of the RCW 106 complex, located in the southern Galactic plane at a distance of 3.8 kpc (Caswell & Haynes 1987); it presents compact far infrared sources (Karnik et al. 2001), intense NH_3 (J,K) = (1,1) line emission (Roman-Lopes et al. 2002) and continuum radio emission at 5 GHz as well as hydrogen recombination lines (Caswell & Haynes 1987).

2. Observations and data reduction

The imaging observations were performed in June 2001 with the Near Infrared Camera (CamIV) of Laboratório Nacional de Astrofísica, Brazil, equipped with a Hawaii 1024x1024 pixel HgCdTe array detector mounted on the 0.6 m Boller & Chivens telescope. The plate scale was 0.47 arcsec/pixel and the mean values of the PSF full width at half maximum (MFWHM) were 1.2, 1.5 and 2 arcsec at the J , H and nbK images, respectively. The observations consisted of $8' \times 8'$ frames in the direction of the IRAS source I16177-5028 using J , H and nbK filters. The narrow band K filter is centered at $2.24956 \mu\text{m}$ with a FWHM of $0.06333 \mu\text{m}$, covering only the continuum emission. The total integration time was 540 s for the J and H bands and 1620 s for the nbK filter, resulting in a sensitivity at 3σ of 17.5, 16.8 and 13.4 magnitudes, respectively. The frames were dithered by 60 arcsec, in order to remove bad pixels, cosmic rays and to eliminate the presence of objects with extended emission on the construction of the sky images. Individual frames were dark subtracted and flat-fielded before being combined. We obtained a set of "dome flats" for each filter using an illuminated white spot in the telescope dome. Sky frames were generated from a median-filtered

set of the flattened frames in each band. To produce a combined image from each dithered set of images, we aligned the frames using the IRAF² subroutines, added the aligned frames and trimmed the resulting image to remove bad pixels at the edges of the frames. We used DAOFIND to locate stars 4σ above the local background and added to the DAOFIND list all stellar objects missed by this routine but found by visual inspection of each image. Because of source confusion within the region, photometry was obtained using the point spread function fitting algorithm ALLSTAR in the DAOPHOT package (Stetson 1987). For the J and H images the adopted PSF fitting radius were 2.0 and 3.2 pixels respectively and the PSF radius was 11 pixels. For the nbK image the PSF fitting radius was 4.2 pixels and the PSF radius was 13 pixels. The local sky was evaluated in an annulus with an inner radius of 8 pixels and a width of 20 pixels. The values of the completeness limits for J , H and nbK bands are 16, 15.5 and 12.2 magnitudes respectively and were derived from the point where the number of detected sources of magnitude m , $N(m)$ deviates from a straight line in the $\log(N)$ versus m diagram as can be seen in figure 1. Photometric calibration was done by observing standards from the list of Elias (1982), at several air masses before and after each set of integrations. Direct equivalence was assumed between our nbK magnitudes and the standard K values.

Photometry from 2MASS All Sky Point Source Catalogue³ in the J , H and K_S filters became available recently. The K_S filter, centered at $2.17\ \mu\text{m}$, has a bandpass of $0.32\ \mu\text{m}$. The completeness limits for this survey are 15.8, 15.1 and 14.3 magnitudes at J , H and K_S , respectively (Egan et al. 2001). Since the 2MASS K_S band photometry has a completeness limit greater than our nbK photometry, we decided to use the 2MASS catalogue astrometry and magnitudes in this filter to study the stellar population. Even though the 2MASS survey was conducted with a 1.3 m telescope, the sensitivity and resolution of our IR camera compensates our smaller collecting area, resulting in more detection in the J and H bands, as it will be shown in section 3.2. For this reason we only used the more sensitive 2MASS K_S photometry.

We also checked the consistence of our photometry comparing it with the data of the 2MASS survey. We took all point sources detected by 2MASS in an area of about 50 square arcmin around IRAS16177-5018 and constructed a list of sources common to both surveys in the three filters. This procedure gave us a total of 612, 781 and 232 sources in the J , H and K bands respectively. We constructed graphs for M_{2mass} versus M_{CamIV} J , H and K magnitudes respectively, which are shown in figure 2. We see a good linear relation between the two systems, with a slope of 1 and a dispersion that increases with the magnitude.

²IRAF is distributed by the National Optical Astronomy Observatories, which is operated by the Assotiation of Universities for Research in Astronomy, Inc. under contract to the National Science Foundation

³<http://www.ipac.caltech.edu/cgi-bin/gator/nph-dd>

3. Results & Discussion

The infrared images, especially in the H , nbK and K_S bands, show the presence of a small infrared nebula ($\sim 70'' \times 70''$ square arcsec) at the IRAS coordinate, with an apparent concentration of embedded stars, suggesting the presence of a cluster. In figure 3 we show a combined pseudoreal colour (J represented in blue, H in green and nbK in red) image of the whole field, and amplified images of the nebular region in the J , H and nbK bands.

In figure 4 we present the $(J - H)$ versus $(H - K_S)$ diagram for all stars detected in the LNA J and H images and in the 2MASS K_S image or only at H and K_S , using the completeness limit for the J magnitude, together with the position of the main sequence, giant branch and reddening vectors for early and late type stars. The majority of the sources have colors of reddened photospheres but some of them appear to the right of the reddening line for early type stars, showing "excess" at $2.2 \mu\text{m}$. When we combine the results shown by the color-color diagram with the spatial distribution of the sources, we verify that all stars situated to the right of the early type reddening vector with $H - K_S \geq 1.0$ are located in the nebular region.

It is well established that very young pre-main sequence objects present large infrared excess due to the presence of warm circumstellar dust. Our result suggests that the stellar population in the direction of the IRAS source is very young, and from their position in the $(J - H)$ versus $(H - K_S)$ diagram they are probably young massive stellar objects.

In order to estimate the amount of interstellar extinction in the direction of the IRAS source we computed the average value of the color excess $E(H - K)$ using the 11 sources from Table 1 (IRS 1, 2, 7, 8, 11, 18, 22, 23, 26, 28 and 31) that lie along the reddening line for early type stars in the color-color diagram. We assumed that the intrinsic $(H - K)_0$ colors are those of luminous early type stars (-0.05 for O6-O8V types as given by Koornneef, 1983). The mean color excess obtained was $\langle E(H - K) \rangle = 1.75$, which for a standard reddening law (Rieke & Lebofsky 1985) corresponds to a median visual extinction $\langle A_V \rangle \approx 2.8$.

3.1. The IRAS source

In Figure 5 we present a contour map constructed from the LNA nbK image, which shows the region around IRAS16177-5018. The IRAS coordinate has an intrinsic error delimited by the ellipse plotted in the figure. Any object inside the ellipse could be identified with the IRAS source and in fact, more than one of these objects may be contributing to the detected infrared flux. A more accurate position for the IR source was obtained from the Midcourse Space Experiment - MSX source catalog⁴. The MSX surveyed the entire Galactic plane within $|b| \leq 5^\circ$ in four mid-infrared spectral bands centered at 8.28, 12.13, 14.65 and 21.34 μm , with image resolution of 20 arcsec and

⁴<http://www.ipac.caltech.edu/ipac/msx/msx.html>

a global absolute astrometric accuracy of about 1.9 arcsec (Price et al. 2001). We found only one MSX source, with coordinates $\alpha(\text{J2000}) = 16^{\text{h}}21^{\text{m}}31.4^{\text{s}}$, $\delta(\text{J2000}) = -50^{\text{d}}25^{\text{m}}04^{\text{s}}$ within the IRAS uncertainty ellipse; it coincides with the star we labeled IRS7 in Table 1. In fact this is the only MSX source in an area of about 9 square arcmin around the IRAS point source with detected flux at the four bands.

In Figure 6 we plotted the near to far-infrared spectral energy distribution of IRS7, without any correction for absorption. We can see that the MSX and IRAS flux densities agree very well at the common wavelengths (12 and 21-25 μm), indicating that only one star is responsible for the IRAS emission. The spectral index in the near and mid-infrared (between 2.2-25 μm), defined as $\alpha = d \log(\lambda F_\lambda) / d \log \lambda$ is $\alpha = 4.78$, characteristic of extremely young stellar objects in a earlier stage of evolution, when the star is deeply surrounded by a thick dusty envelope.

We integrated the observed flux density between 1.25 and 100 μm and, assuming a distance of 3.8 kpc, we obtained a luminosity $L = 2.8 \times 10^5 L_\odot$. Since most of the energy is emitted in the infrared, this can be considered a lower limit to the bolometric luminosity of the embedded star, reprocessed by a dusty envelope. PMS models (Iben 1965) show that massive stars (above 9 M_\odot) evolve at constant luminosity from the Hayashi track to the Main-Sequence. Therefore, the measured luminosity gives directly a lower limit to the stellar mass of 42 M_\odot , corresponding to a ZAMS star earlier than O5.5 (Hanson et al. 1997), independent of its PMS evolutionary stage.

3.2. Cluster Population

In order to examine the assumption that a cluster of embedded young stars is present in the core of the molecular cloud, we analyzed the stellar population in two delimited regions; one that we labeled "nebulae" that contains the cluster and another that we labeled "control", as illustrated in Figure 7. In that figure we represented the position of all objects detected in the H band by crosses. We can see that the small region labeled "cluster region" show a concentration of sources. As mentioned in section 3, all the sources with excess emission at 2.2 μm belong to the nebular region, which has an area about 1 square arcmin ($\sim 1 \times 1$ sq parsec at a distance of 3.8 kpc), compatible with the sizes of other stellar clusters studied with near infrared arrays (Persi et al. 1994; Tapia et al. 1996; Persi et al. 1997).

In order to separate the cluster sources not detected at J band from the field stars, we constructed a comparative $H - K_S$ color distribution diagram for the control and "cluster" regions (with the counts for the control region normalized to the "cluster" region area), shown in figure 8. From this diagram we can also see the existence of an excess of sources with $H - K_S > 1.0$ in the direction of the nebulae.

Using these results, the following criteria was used to select the "cluster member candidates" for the nebulae region: a) sources with $H - K_S > 1.0$ that lie to the right or on the reddening vector for early type stars in the color-color diagram; b) sources with $H - K_S > 1.0$ not detected at the J

band and c) sources detected only at K_S band. For the b) and c) criteria, the contamination from background stars, mainly late-type giants, should be very small. In fact for an average extinction A_V of 28 magnitudes, the extinction in the K band A_K is about 3.1 magnitudes (using the interstellar reddening law taken from Rieke & Lebofsky, 1985), and for a distance to the cloud of 3.8 kpc, these sources would have $K > 16$. Table 1 shows the coordinates and photometry of all selected sources (J and H from both LNA and 2MASS and K_S and coordinates from 2MASS). From the 41 stars with measured K_S magnitudes we were able to measure the LNA magnitudes in 35 of them at H and 22 at J bands, while the 2MASS survey only detected 20 objects at H and 6 at J bands.

Further information about the nature of the selected objects in Table 1 can be extracted from K_S versus $(H - K_S)$ color-magnitude diagram shown in Figure 9. The locus of the main-sequence for class V stars it is also plotted, with the position of each spectral type earlier than A0 V indicated by filled circles. The intrinsic colors were taken from Koornneef (1983) while the absolute K magnitudes were calculated from the absolute visual luminosity for ZAMS taken from Hanson et al. (1997), for a distance of 3.8 kpc (Caswell & Haynes). The reddening vector for a ZAMS B0 V star, taken from Rieke & Lebofsky (1985), is shown by the dashed line with the positions of visual extinctions $A_V = 10, 20$ and 30 magnitudes indicated by filled circles. From this diagram we can see that the majority of sources can be classified as reddened massive stars earlier than spectral type B5, forming an O-B cluster embedded in the molecular cloud. However, the spectral types inferred from the color-magnitude diagram are only upper limits when the stars present emission "excess" in the NIR.

We made a crude estimate of the star formation efficiency using the mass of gas measured by Karnik et al. (2001). They mapped the RCW 106 region at 150 and 210 μm and detected a compact region in the direction of the IRAS source 16177-5018. They modeled the observed mid and far-infrared SED assuming a constant gas to dust relation $M_{\text{gas}}/M_{\text{dust}} = 100$ and from the integrated luminosity about $10^5 L_\odot$ they obtained a mass of dust $M_{\text{dust}} \approx 30 - 35 M_\odot$ resulting in a mass of gas $M_{\text{gas}} \approx 3000 - 3500 M_\odot$. From this value we estimated a lower limit to the star formation efficiency (*SFE*), using the lower limit to the number of cluster members detected as 41 and an average stellar mass of $15 M_\odot$, which corresponds to a B0 V star (Hanson et al. 1997):

$$\text{SFE} = \frac{M_{\text{stars}}}{M_{\text{gas}} + M_{\text{stars}}} = 0.17 \quad (1)$$

This is a lower limit because the mass of gas assumed for the nebular region may be overestimated since it can include a larger volume than our star forming region and also because stars fainter than our detection limit are not included.

We also estimated the number of Lyman-continuum photons produced in the star forming region, from the spectral types of the stars that do not show "excess" in the color-color diagram, using the relation between spectral type and number of Lyman-continuum photons given by Hanson et al. (1997). We obtained 1.6×10^{50} photons s^{-1} .

3.3. The infrared nebula

In figure 10 we shown contour maps of the infrared nebulae region at J , H and nbK bands obtained from our infrared images. The contours were calibrated in flux with the values starting at 0.18, 0.48 and 2.8×10^{-4} Jy/beam respectively. From the nbK contour map we estimated a lower limit to the flux density of the emission nebula in the K band by measuring the area between contours and multiplying by the value of the corresponding flux density per unit area and we found $S(K) = 0.62$ Jy. Assuming that the emission process is thermal bremsstrahlung from an optically thin region, we can compare the IR with the radio flux density at 5 GHz given by Caswell & Hynes (1987) to obtain an upper limit to the K -band absorption. Assuming constant density and temperature across the cloud and local thermodynamic equilibrium, the flux density $S(\nu)$ due to free-free emission can be written as:

$$S(\nu) = \tau_\nu B_\nu(T) \Omega \quad (2)$$

where τ_ν is the optical depth at frequency ν , $B_\nu(T)$ is the Planck function

$$B_\nu(T) = \frac{2h\nu^3}{c^2} \frac{1}{\exp(k\nu/kT) - 1} \quad (3)$$

and Ω is the solid angle of the source given by:

$$\Omega = \pi(L/2D)^2 \quad (4)$$

where L is the diameter of the ionized cloud and D the distance to the observer. The optical depth at a given frequency ν is:

$$\tau_\nu = \alpha_{\text{ff}} L \quad (5)$$

where α_{ff} is the free-free absorption coefficient (cgs) taken from Rybick (1979):

$$\alpha_{\text{ff}} = \frac{3.7 \times 10^8 [1 - \exp(-h\nu/kT)] (n_e n_i) g_{\text{ff}}(\nu, T)}{\nu^3 Z^{-2} T^{1/2}} \quad (6)$$

$g_{\text{ff}}(\nu, T)$ is the Gaunt factor obtained from Clayton (1968)

For two frequencies ν_1 and ν_2 the ratio of the corresponding flux densities $S(\nu_1)$ and $S(\nu_2)$ may be calculated from:

$$\frac{S(\nu_1)}{S(\nu_2)} = \exp[h(\nu_2 - \nu_1)/kT] \frac{g_{\text{ff}}(\nu_1, T)}{g_{\text{ff}}(\nu_2, T)} \quad (7)$$

For a flux density in the 5 GHz continuum of 32.4 Jy and an electron temperature $T_e = 6300$ K, as given by Caswell & Haynes (1987) we find an expected flux density at the K band of 11.5 Jy. The measured value of 0.62 Jy gives an upper limit to the K band absorption of 3.1 magnitudes. Using the interstellar extinction law given by Rieke & Lebofsky (1985) we obtained a visual extinction $A_V \approx 27.7$ in very good agreement with the value obtained in section 3.0 from the median ($H - K$) color excess.

We observe that it is possible that the detected infrared flux at $2.2\mu\text{m}$ has a contribution from light scattered by dust, but taking into account that the ionized region detected at radio wavelengths coincides with the near infrared nebulae and the high number of massive stars inferred from the color-magnitude diagram, we believe that the major contribution to the K band integrated flux is probably due to free-free emission from the ionized region.

We also obtained the number of ionizing Lyman continuum photons N_{Ly} from the radio continuum flux density using the expression derived by Rubin (1968):

$$N_{Ly} = \frac{5.99 \times 10^{47} S(\nu) D^2 T_e^{-0.45} \nu^{0.1}}{1 + f_i [He^+ / (H^+ + He^+)]} \quad (8)$$

where ν is in MHz and f_i is the fraction of helium recombination photons that are energetic enough to ionize hydrogen ($f_i \approx 0.65$). We assumed, as in Simpson & Rubin (1990) the ratio $He/H = 0.1$ and the average volume of He^+ as half the volume of H^+ . Using Equation 7 we found $N_{Ly} \sim 5.2 \times 10^{49}$ photons s^{-1} . This value is compatible with the number of Lyman continuum photons available from the main sequence stars derived in the previous section.

3.4. Conclusions

Near-IR imaging photometry in the direction of the IRAS source 16177-5018 revealed a young massive stellar cluster and its associated HII region embedded in a dense molecular cloud. We detected 41 cluster member candidates concentrated in an area of 1 square parsec, but probably other less massive sources were missed because the completeness limit.

The NIR counterpart of the IRAS point source was identified using more accurate positions from the MSX catalogue. This source has a near-mid spectral index $d \log(\lambda F_\lambda) / d \log \lambda = 4.78$ indicating that the IRAS source is very young, with a lower limit to the bolometric luminosity inferred from the integrated near to far-infrared flux density of about $2.8 \times 10^5 L_\odot$, which corresponds to a $42 M_\odot$ star.

The average absorption found for the embedded early type stars ($A_V \sim 28$) coincides with the absorption of the HII region, derived by comparing the integrated extended flux density at the K band to what is expected at this band from the observed radio emission.

The number of Lyman continuum photons expected from the 11 stars that lie along the reddening line for early-type stars about $1.3 \times 10^{50} s^{-1}$, enough to produce the 5 GHz flux density and near IR emission, assumed to be originated by free-free emission.

This work was partially supported by the Brazilian agencies FAPESP and CNPq. We acknowledge the staff of Laboratório Nacional de Astrofísica for their efficient support and to F. Jablonsky who was the PI of the CamIV project. We also thank the anonymous referee for constructive suggestions that improved the quality of this paper. This publication makes use of data products

from the Two Micron All Sky Survey, which is a joint project of the University of Massachusetts and the Infrared Processing and Analysis Center/California Institute of Technology, funded by the National Aeronautics and Space Administration and the National Science Foundation.

REFERENCES

- Bronfman, L. Nyman, L. A., May, J. 1996, A&AS, 115, 81
- Carpenter, J. M., Meyer, M. R., Dougados, C., Strom, S.E., Hillenbrand, L.A. 1997, AJ, 114, 198
- Caswell, J. L., Haynes, R. F. 1987, A&A, 171, 261
- Clayton, D. D. 1968, Principles of Stellar Evolution and Nucleosynthesis, ed. McGRAW-HILL. San Francisco
- Egan, M. P., Dyk, S. D. V., Price, S. D. 2001, AJ, 122,1844
- Eiroa, C., Casali, M. M. 1992, A&A, 262, 468
- Elias, J. H. 1982, AJ, 87, 1029
- Hanson, M. M., Howarth, I. D., Conti, P. S. 1997, ApJ, 489, 718
- Iben, I. Jr. 1965, ApJ, 141, 993I
- Karnik, A. D., Ghosh, S. K., Rengarajan, T. N., Verma, R. P. 2001, MNRAS, 326, 293
- Koornneef, J. 1983, A&A, 128, 84
- Lada, C. J. 1987, IAUS, 115, 1L
- Lada, J. C., Adams, F. C. 1992, ApJ, 393, 278
- Mathis, J. S. 1990, ARA&A, 28, 37
- Persi, P., Roth, M., Tapia, M., Ferrari-Toniolo, M., Marenzi, A. R. 1994, A&A, 282, 474
- Persi, P., Felli, M., Lagage, P. O., Roth, M., Testi, L. 1997, A&A, 327, 299
- Price, S. D., Egan, M. P., Carey, S. J., Mizuno, D. R., Kuchar, T. A. 2001, AJ, 121, 2819
- Rieke, G. H., Lebofsky, M. J. 1985, ApJ, 288, 618
- Roman-Lopes, A., Abraham, Z., Caproni, A., Lépine, J. R. D. 2002, IAUS, 206, 244
- Rubin, R. H. 1968, ApJ, 154, 391R
- Rybicki, G. B., Lightman, A. P. 1979, Radiative Processes in Astrophysics, ed. JOHN WILEY & SONS, New York

Simpson, J. P., Rubin, R. H. 1990, ApJ, 354, 165

Spitzer, L. 1978, Physical Processes in the Interstellar Medium, ed. Wiley, New York

Stetson, P. B., 1987, PASP, 99, 191

Tapia, M., Persi, P., Roth, M. 1996, A&A, 316, 102

Wood, D. O. S., Churchwell, E. 1989, ApJ, 340, 265

Table 1. List of the selected near-infrared sources

IRS	α (J2000)	δ (J2000)	J_{camiv}	σ	J_{2mass}	σ	H_{Camiv}	σ	H_{2mass}	σ	K_{2mass}	σ
1	16:21:31.60	-50:25:08.3	16.65	0.15	—	—	12.73	0.08	12.76	0.08	10.21	0.08
2	16:21:31.86	-50:25:04.7	16.49	0.11	—	—	13.23	0.09	13.13	0.11	10.92	0.10
3	16:21:31.35	-50:24:57.9	—	—	—	—	14.98	0.13	—	—	11.25	0.12
4	16:21:33.03	-50:25:04.6	—	—	—	—	15.02	0.10	—	—	11.37	0.07
5	16:21:32.21	-50:25:09.6	—	—	—	—	15.66	0.12	—	—	11.39	0.11
6	16:21:30.77	-50:24:57.1	—	—	—	—	15.11	0.11	—	—	11.44	0.11
7	16:21:31.34	-50:25:04.1	17.37	0.25	—	—	13.88	0.05	13.73	0.14	11.45	0.09
8	16:21:30.56	-50:25:19.2	18.07	0.30	—	—	14.23	0.09	14.14	0.13	11.56	0.12
9	16:21:33.94	-50:24:31.5	16.39	0.11	—	—	13.27	0.05	13.31	0.04	11.66	0.04
10	16:21:31.12	-50:24:51.9	17.30	0.27	—	—	14.87	0.08	—	—	11.68	0.13
11	16:21:30.45	-50:25:04.2	15.75	0.13	15.65	0.10	13.46	0.05	13.33	0.11	11.73	0.13
12	16:21:30.52	-50:25:14.5	16.15	0.14	16.19	0.11	14.70	0.06	14.68	0.12	11.89	0.12
13	16:21:30.89	-50:25:07.2	17.56	0.32	—	—	14.50	0.06	14.53	0.13	11.96	0.09
14	16:21:31.01	-50:25:26.0	—	—	—	—	15.54	0.12	—	—	12.09	0.13
15	16:21:31.10	-50:25:15.1	—	—	—	—	14.72	0.08	—	—	12.24	0.15
16	16:21:28.02	-50:24:42.6	15.21	0.08	15.23	0.06	13.30	0.05	13.34	0.05	12.39	0.05
17	16:21:30.38	-50:25:25.1	—	—	—	—	15.86	0.10	—	—	12.46	0.17
18	16:21:28.79	-50:24:09.9	16.43	0.14	—	—	13.97	0.07	13.92	0.06	12.50	0.07
19	16:21:31.84	-50:24:45.9	—	—	—	—	15.35	0.07	15.32	0.18	12.51	0.10
20	16:21:29.53	-50:25:00.9	16.69	0.13	—	—	14.59	0.08	—	—	12.51	0.10
21	16:21:30.09	-50:25:23.3	16.72	0.11	—	—	15.28	0.06	—	—	12.64	0.14
22	16:21:29.50	-50:24:44.9	15.29	0.08	15.21	0.06	13.57	0.03	13.66	0.03	12.73	0.08
23	16:21:29.39	-50:24:49.4	16.94	0.17	—	—	14.24	0.07	14.44	0.06	12.82	0.03
24	16:21:30.91	-50:24:40.7	17.71	0.28	—	—	15.07	0.04	15.08	0.13	12.88	0.16
25	16:21:26.42	-50:24:47.0	16.87	0.13	—	—	14.38	0.05	14.25	0.11	13.09	0.09
26	16:21:28.48	-50:24:34.3	16.45	0.08	—	—	14.39	0.05	14.34	0.10	13.10	0.11
27	16:21:29.46	-50:25:16.7	15.59	0.08	15.76	0.07	14.60	0.05	14.53	0.08	13.45	0.18
28	16:21:29.64	-50:24:02.4	16.63	0.13	—	—	14.64	0.05	14.74	0.15	13.57	0.11
29	16:21:31.68	-50:25:31.8	—	—	—	—	15.45	0.07	—	—	13.58	0.14
30	16:21:33.41	-50:25:18.5	—	—	—	—	15.56	0.06	—	—	13.63	0.06
31	16:21:28.92	-50:25:00.1	16.71	0.11	—	—	14.73	0.05	14.80	0.13	13.73	0.13
32	16:21:34.11	-50:25:27.9	—	—	—	—	16.52	0.11	—	—	13.80	0.15
33	16:21:27.95	-50:26:18.5	—	—	—	—	14.97	0.07	—	—	13.93	0.11
34	16:21:33.66	-50:25:31.3	16.01	0.13	15.95	0.10	15.25	0.10	15.10	0.14	14.04	0.18
35	16:21:34.86	-50:24:36.6	—	—	—	—	17.35	0.20	—	—	14.26	0.09
36	16:21:27.82	-50:26:21.7	—	—	—	—	—	—	—	—	13.38	0.13
37	16:21:33.51	-50:25:46.5	—	—	—	—	—	—	—	—	13.51	0.16
38	16:21:33.92	-50:25:41.4	—	—	—	—	—	—	—	—	13.56	0.12
39	16:21:35.38	-50:24:59.6	—	—	—	—	—	—	—	—	13.89	0.05
40	16:21:35.95	-50:26:08.4	—	—	—	—	—	—	—	—	14.11	0.07
41	16:21:28.43	-50:25:35.6	—	—	—	—	—	—	—	—	14.87	0.15

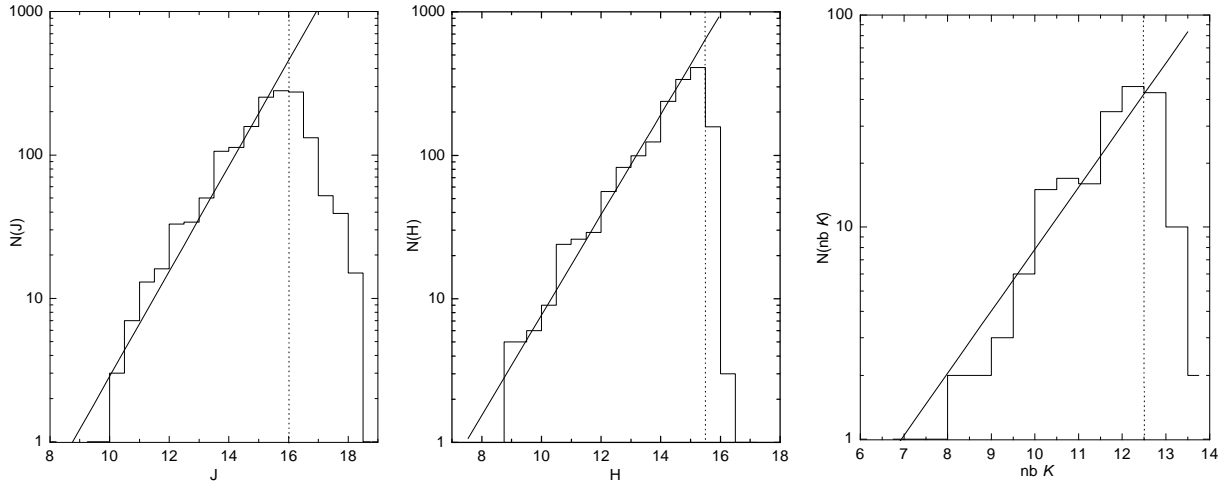


Fig. 1.— Histograms of J (a), H (b) and nbK (c) magnitude counts. The completeness limits are indicated by the vertical dotted lines.

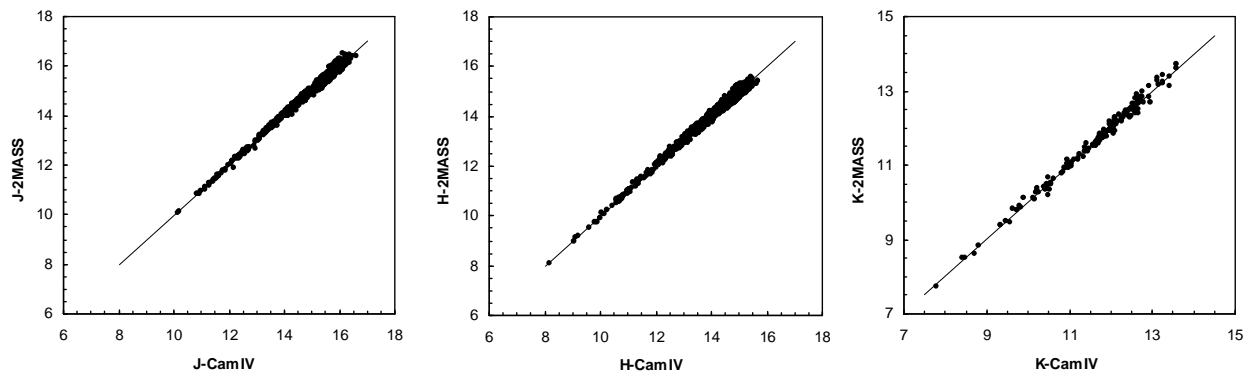


Fig. 2.— The magnitudes comparative diagram $M_{JHK}(2MASS) \times M_{JHK}(CamIV)$. The continuous line shows the relation expected if the two photometric systems were equal.

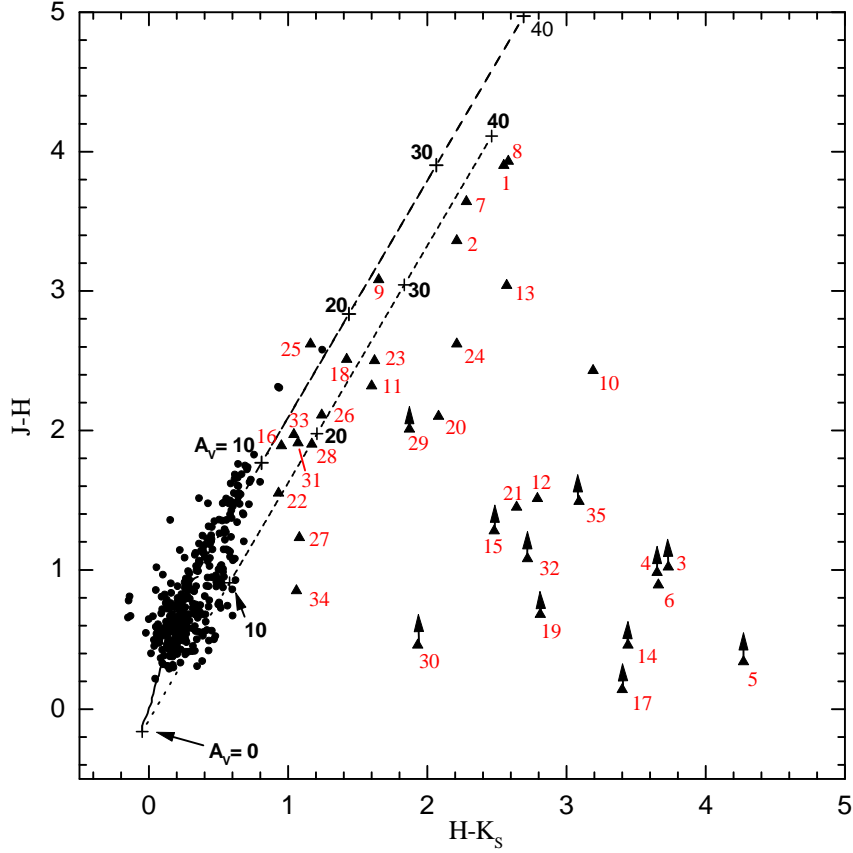


Fig. 3.— Color-color diagram of all sources detected at the three passbands. The locus of the main sequence and giants branch are shown by the continuous lines taken from Koornneef (1983), while the two parallel lines (dashed and dotted) follow the reddening vectors taken from Rieke & Lebofsky (1985). The location (crosses) of $A_V = 0, 10, 20, 30$ and 40 magnitudes of visual extinction are indicated by black bold numbers. We also plotted the sources only detected at H and 2MASS K_S images using the completeness limit of the J photometry (about 16 mag). These sources have lower limit to the J-H color indicate by arrows. The cluster members candidates taken from table 1 are labeled by the red numbers.

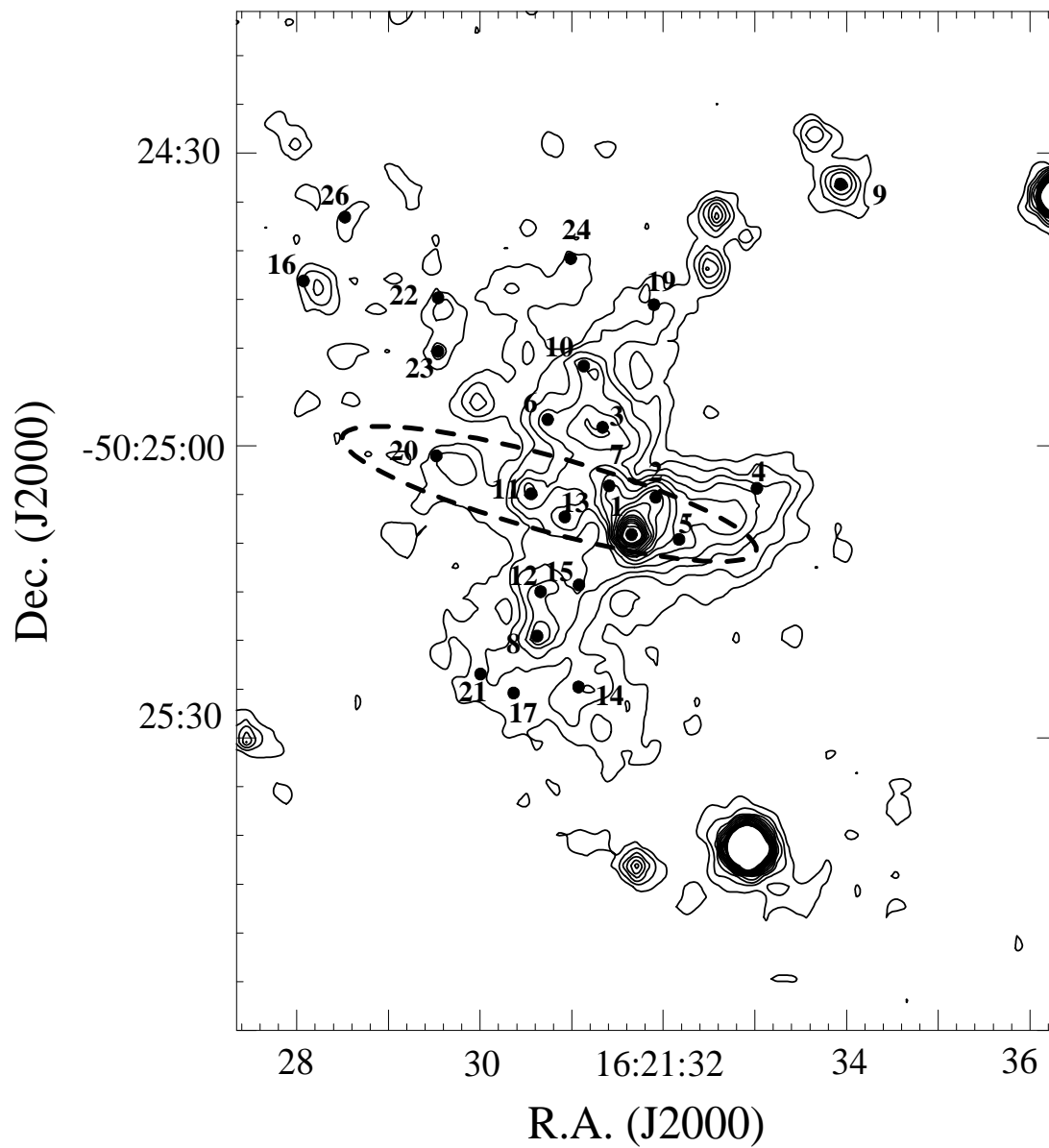


Fig. 4.— nbK band contour map of the infrared nebulae associated with IRAS16177-5018. The contours start at 1.8×10^{-4} Jy/beam, with the same intervals (the beam size is 2×2 pixels). The positions of selected infrared sources taken from table 1 are indicated by black numbers. It is also indicated the location of the IRAS coordinate ellipse error (black dotted line).

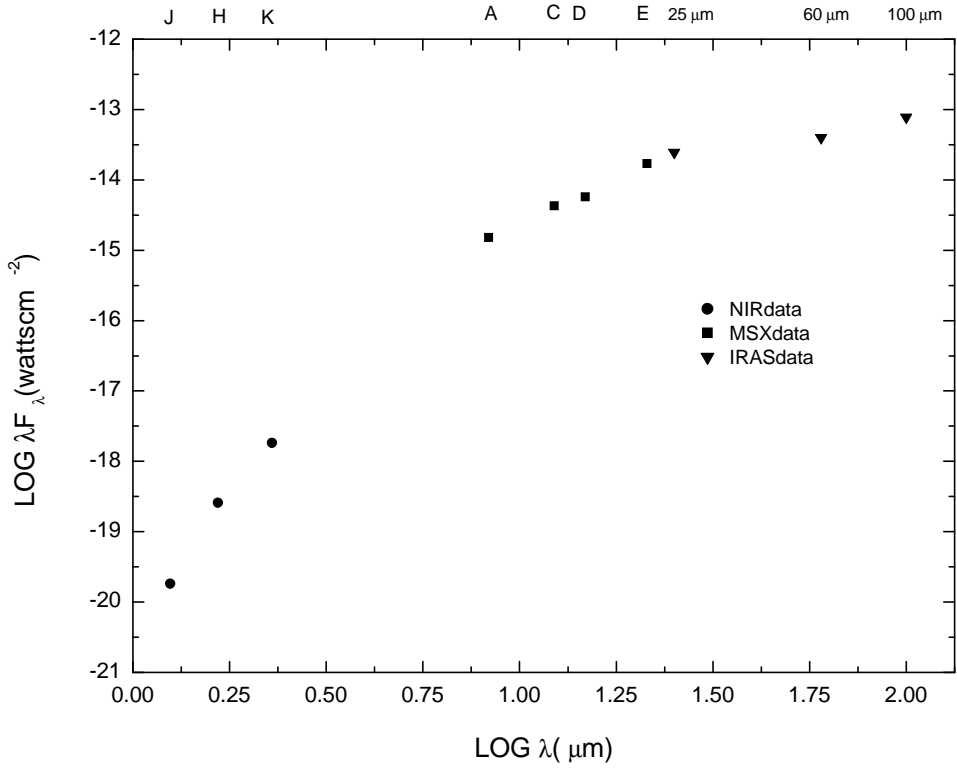


Fig. 5.— Spectral energy distribution of the IRS7 infrared source. The flux for the three near infrared bands (filled circles) were taken from our survey. The mid infrared data (filled squares) were taken from *MSX catalogue* (bands A=8.28 μm , C=12.13 μm , D=14.65 μm and E=21.34 μm) while the far infrared data (filled down triangles) were taken from IRAS point source catalogue.

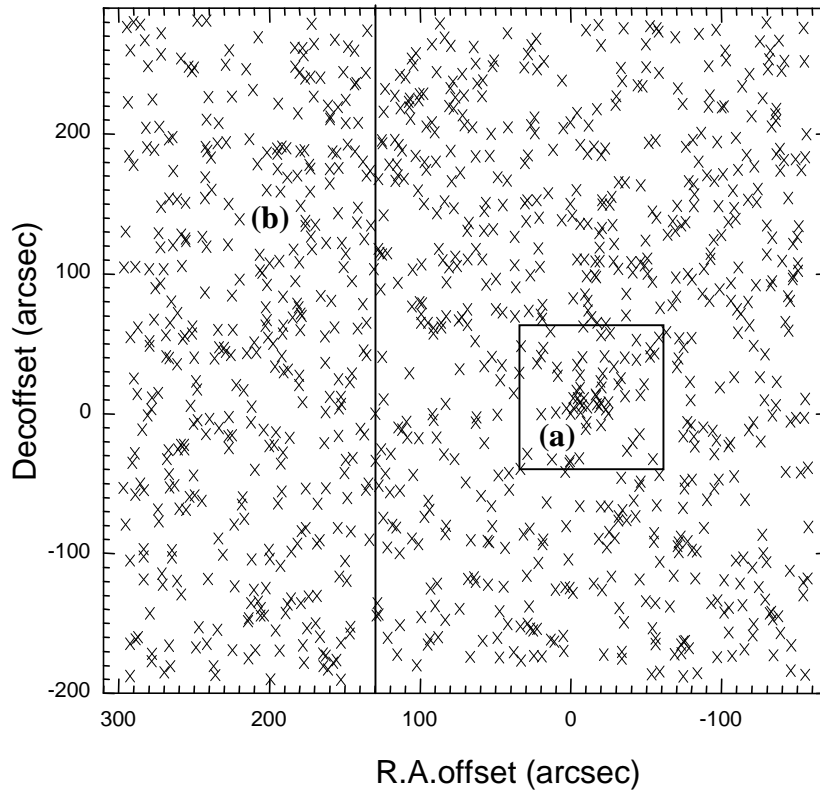


Fig. 6.— Diagram of the spacial distribution of sources detected at LNA’s H band . The two comparative regions **a** (nebulae) and **b** (control) are delimited by the vertical continuum line. The ”cluster region” area is delimited by the dotted square at the up right side.

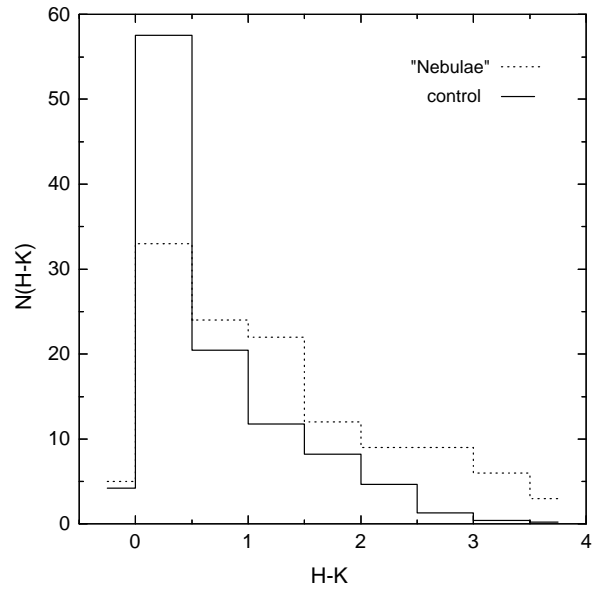


Fig. 7.— Comparative diagram of the distribution of the $H - K$ color for the "control" (continuous line) and "nebulae" (dotted line) areas .

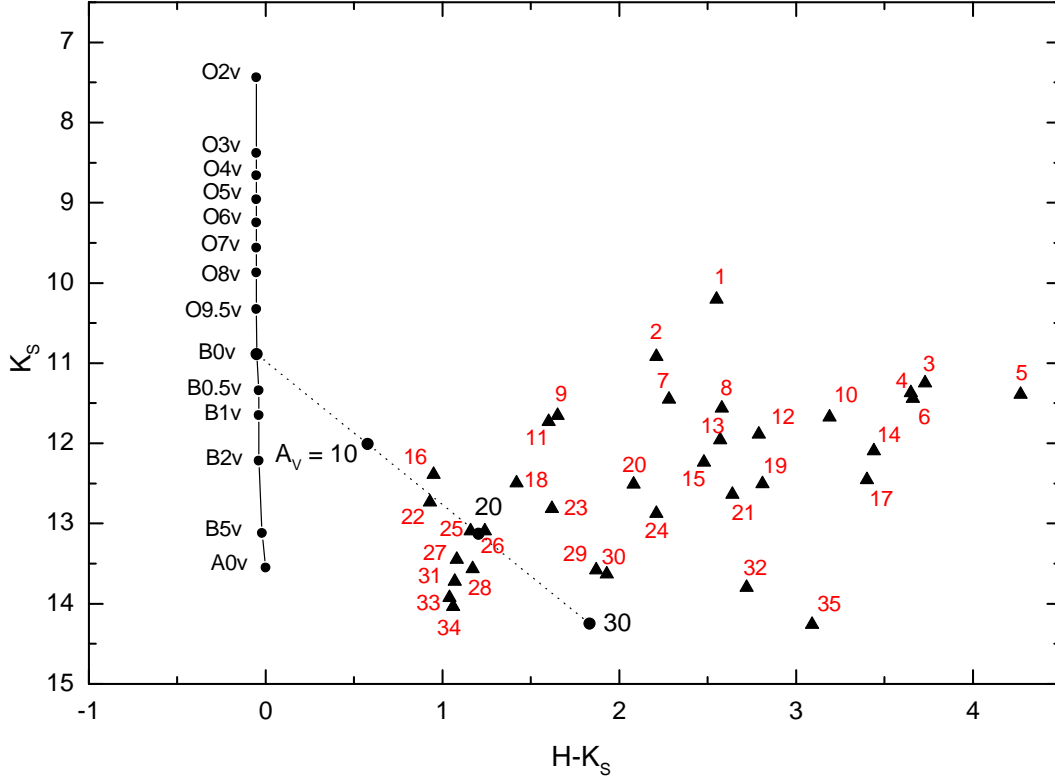


Fig. 8.— $K_S \times (H - K_S)$ color-magnitude diagram of the selected sources in table 1. The locus of the main sequence (dwarfs) at 3.8 kpc is shown by the continuous line. The intrinsic colors were taken from Koornneef (1983) while the absolute K magnitudes were calculated from the absolute visual luminosity for ZAMS taken from Hanson et al. (1997). The reddening vector for a B0 ZAMS star (dotted line) was taken from Rieke & Lebofsky (1985); Also are indicated the location (filled circles) of $A_V = 10, 20$ and 30 magnitudes of visual extinction. The sources IRS1-IRS35 are labelled by red numbers.

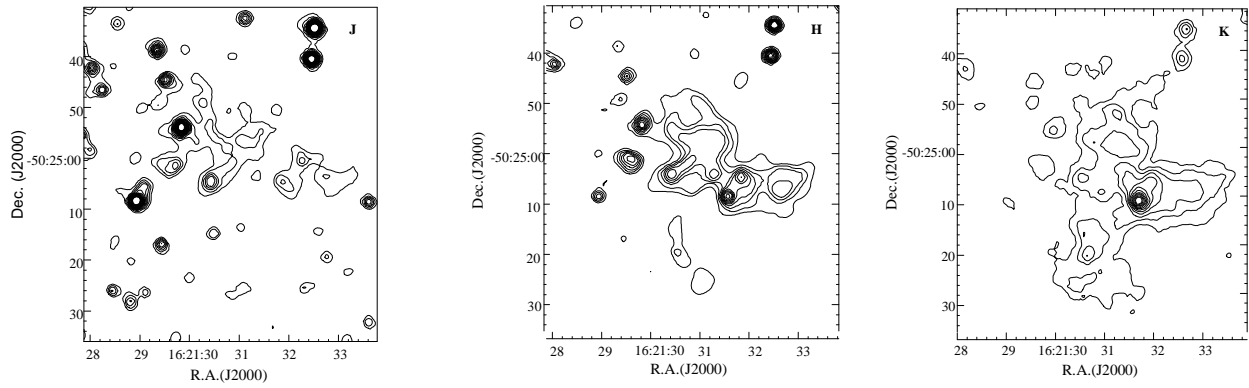


Fig. 9.— J, H and nbK contour maps of the infrared nebulae region. The contours start at 1.8×10^{-5} Jy/beam in *J*, 4.8×10^{-5} Jy/beam in *H* and 2.8×10^{-4} Jy/beam in nb*K*, and are spaced by the same fluxes per beam (a beam is 2×2 pixels).

This figure "Roman-Lopes.fig3.jpg" is available in "jpg" format from:

<http://arxiv.org/ps/astro-ph/0306495v1>